Lithium-ATP: structure characterization and lithium binding

Anat Haimovich and Amir Goldbourt

School of Chemistry, Tel Aviv University, Tel Aviv 6997801, Israel

Abstract

Lithium is a leading drug for the treatment of bipolar disorder and affects many biochemical pathways via inhibition of phosphatases and kinases. Lithium can replace magnesium cations in enzymes and small molecules, among them ATP. Here we extract the binding environment of lithium in LiATP. Using a multi-nuclear solid-state NMR approach, we determine that lithium coordinates with the first (P_α) and second (P_β) phosphates of one ATP molecule, and with the second ($P_{\beta'}$) phosphate of a second ATP molecule in the unit cell. The Li-P distance is 3 Å. The fourth coordination is probably to water. We suggest that the phosphate chains are non-linear and that P_γ of one ATP molecule resides in between $P_{\alpha'}$ and $P_{\gamma'}$ of a second ATP molecule. Despite the use of excess lithium in the preparations, sodium ions still remain bound to the sample, at distances of 4.3-5.5 Å from Li, and coordinate P_γ, $P_{\gamma'}$, and P_α.

Introduction

The adenosine triphosphate (ATP) molecule is of paramount importance, enabling myriad processes including energy transport within cells. It takes part in many cellular processes including signal transduction. It is the substrate for GSK-3β (glycogen synthase kinase-3β), an enzyme which is involved in many signaling pathways and has been linked with the pathogenesis of several diseases including type 2 diabetes, Alzheimer's disease and bipolar disorder.[1,2] ATP is composed of a purine base called adenine, a ribose, and three phosphate groups. ATP binds to a variety of metal ions, and its metal bound form is the substrate for numerous enzymes. Physiologically, Mg^{2+} is the most relevant metal ion that binds ATP.

Lithium has many biological molecular targets, including molecules that are neurotrophic and molecules related with important signal transduction pathways.[3] It is an inhibitor of phosphatases and kinases, and it interacts with phosphorylated substrates such as ATP, the biological substrate for GSK-3β (in the magnesium bound form) thus causing its inhibition. Lithium enters the cells via voltage-sensitive sodium channels and can affect intracellular sodium and calcium levels.[4]

The structure and binding of metal complexes of ATP has been studied extensively, and the association constants of different metals to ATP were measured by various

methods to some diversity.[5–14] These solution state studies report on a 1:1 ionic complex formation, dominated by the $MgATP^{2-}$ species. However, the existence of the neutral Mg_2ATP complex was also observed[8,12] and the possible formation of the complex, $Mg(ATP)_2^{6-}$ was suggested.[7] Measurements have shown that for the $MATP^{2-}$ complex (M≡Metal), among divalent cations Mg^{2+} is a strong, but not the strongest, binder,[5,6,8,10,11]. Among monovalent cations such as Li^+, Na^+, and K^+, Li^+ has the strongest binding affinity. It was also determined that monovalent cations compete with magnesium binding to ATP.[10]

The ATP molecule has been studied by various NMR techniques. Metal binding has been shown to affect ^{31}P chemical shifts and ^{31}P–^{31}P scalar couplings in solution.[12–20] Ramirez et al. suggested that changes in the chemical shifts resulted from conformational changes of the phosphate chain and were not necessarily indicative of metal binding to a specific phosphate group.[17] On the other hand, Haake et al. concluded that changes in ^{31}P chemical shifts must only be due to direct association with the metal.[13] Solid state Magic-angle spinning (MAS) ^{31}P NMR studies of disodium-ATP[20,21] related changes in the phosphorous spectra also to the hydration state.

Sodium ATP structural crystallographic studies[22–24] in the solid state revealed two ATP molecules in the asymmetric unit, with four chemically inequivalent sodium sites and six water molecules. Two of the sodium sites form a dimer coordinating to the phosphate oxygens and a base nitrogen of both ATP molecules. The other two link the ATP dimers in the extended structure. The phosphate chains have a folded conformation and form partial helices; molecule A forms a left handed helix and molecule B forms a right handed helix. The ribose rings also have different conformations; molecule A has an N-type sugar pucker while molecule B has an S-type sugar pucker. The adenine bases are stacked almost parallel to each other. The existence of four inequivalent sodium sites in sodium ATP has also been identified in ^{23}Na multiple-quantum MAS (MQMAS) NMR studies combined with quantum mechanical calculation methods.[25–28]

Magnesium ATP could only be crystalized with bis(2-pyridyl)amine (bipyam) creating $[Mg(H_2O)_6][Hbipyam]_2[Mg(HATP)_2]\cdot nH_2O$ complexes.[29–31] Mg occupies two inequivalent sites, where one Mg^{2+} cation forms an ATP-metal complex and the other binds six water molecules. The ATP-metal complex has an octahedral geometry with the metal bound to all phosphate groups, three from each ATP molecule. No bonding interactions were observed with the purine base or the ribose. ^{25}Mg MQMAS NMR studies also revealed the existence of two magnesium sites.[32] The phosphate chains in MgATP also have a folded conformation and are part of a network of

hydrogen bonds formed with the metal-water complex, the adenine nitrogens, the ribose hydroxy oxygens and free water. Both ribose rings show an S-type sugar pucker conformation. The purine base has strong stacking interactions with the bipyam molecules and not with other bases. The metal-water complex was suggested to play a role in phosphoryl transfer due to its coordination with the phosphates chain.

Evidence for competition in solution between Li^+ and Mg^{2+} for binding sites in ATP was obtained using fluorescence, Isothermal titration calorimetry (ITC), spin-lattice ^7Li T_1 relaxation time measurements and ^{31}P NMR.[10,14,19,33] It was argued that binding of the metals to the base or sugar moieties was negligible and that Li^+ and Mg^{2+} compete for phosphate binding sites. Furthermore it was shown that magnesium affinity is greater than that of lithium and that lithium binding constants to the phosphate group were somewhat greater in the presence of magnesium. While both LiATP and Li_2ATP species exist, at pH>7 the Li_2ATP species predominates. Both Mg^{2+} and Li^+ were said to bind to all three phosphate groups. A recent ^7Li relaxation study in solution suggested that lithium binds MgATP to form a physiologically relevant MgLiATP complex, where Mg^{2+} coordinates to P_β, P_γ, and water molecules, and Li^+ coordinates to P_γ and water molecules (one bridging Mg^{2+}).[34] Free energy calculations on MgLiATP complexes concluded that Mg^{2+} binds all phosphates, Li^+ binds P_β and P_γ, and the two metals are linked by a hydroxide bridge. It was also determined that lithium binding to MgATP did not significantly alter the complex conformation implicating on the biological action of lithium.[35]

Here we utilize a multi-nuclear MAS ssNMR approach to study a lithium-ATP-water complex, prepared from sodium-ATP, in order to find the lithium binding site. We show that there are two inequivalent molecules in the unit cell, and we suggest a model for lithium binding that involves P_α and P_β of one ATP molecule, and $P_{\beta'}$ of the second ATP molecule. Excess lithium does not replace all sodium ions in the complex, which bind both $P\gamma$ phosphates.

Results & Discussion

Effects of lithium binding on the triphosphate chain:

The ^{31}P CPMAS spectrum of the LiATP complex, prepared according to a protocol which produced a trihydrate NaATP, is shown in **Figure 1**. The six ^{31}P signals belong to two ATP molecules occupying the asymmetric unit, as observed before for sodium ATP. Also, the spectral features are in agreement with the trihydrate form observed for sodium ATP[20,21].

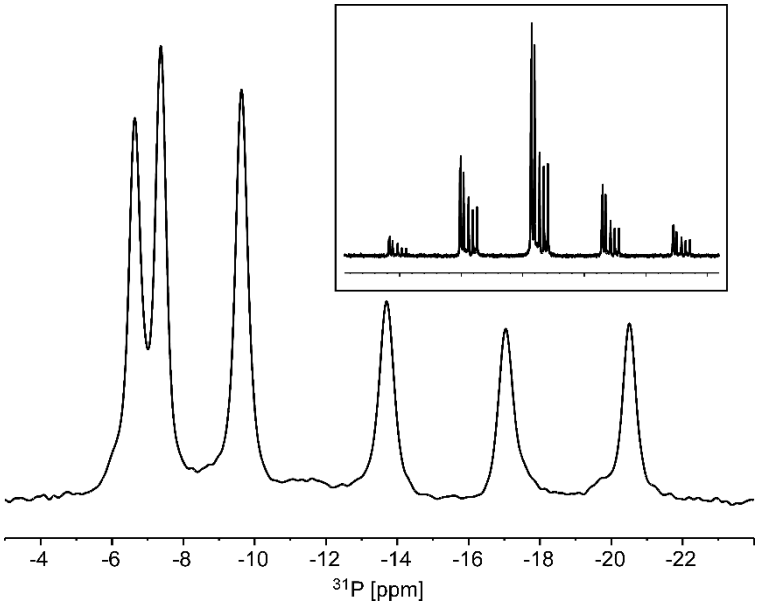

Figure 1: $^{1}H-^{31}P$ CPMAS center-band spectrum of LiATP. The full spectrum is shown in the inset.

In order to assess the effect of lithium binding on the spectrum, the signals need to be assigned to particular phosphate atoms. We therefore performed $^{31}P-^{31}P$ homonuclear DARR (dipolar assisted rotational resonance[36]) correlation experiments using two mixing times. A DARR experiment conducted with a mixing time of 15 ms (DARR15) is shown in **Figure 2a**. It mainly establishes connectivities within each individual ATP molecule. This approach is similar to the one used to characterize NaATP[21]. With this spectrum it was possible to identify each molecule unequivocally. By comparison to prior studies, we know that γ-phosphates are located at a low-field (high-frequency) position, followed by the α-phosphates and then by the β-phosphates. The locations of the phosphates within the molecule are shown in **Scheme 1**. The relatively strong γ-α correlation suggests that also here, as in the case of sodium and magnesium ATP, the phosphate moiety adopts a bent conformation. Moreover, it is also possible to observe the inter-molecular correlations $P_{\alpha}-P_{\gamma'}$ (in asterisks), while other inter-molecular correlations were significantly weaker. This cross-peak already suggests a form of packing of the two inequivalent molecules.

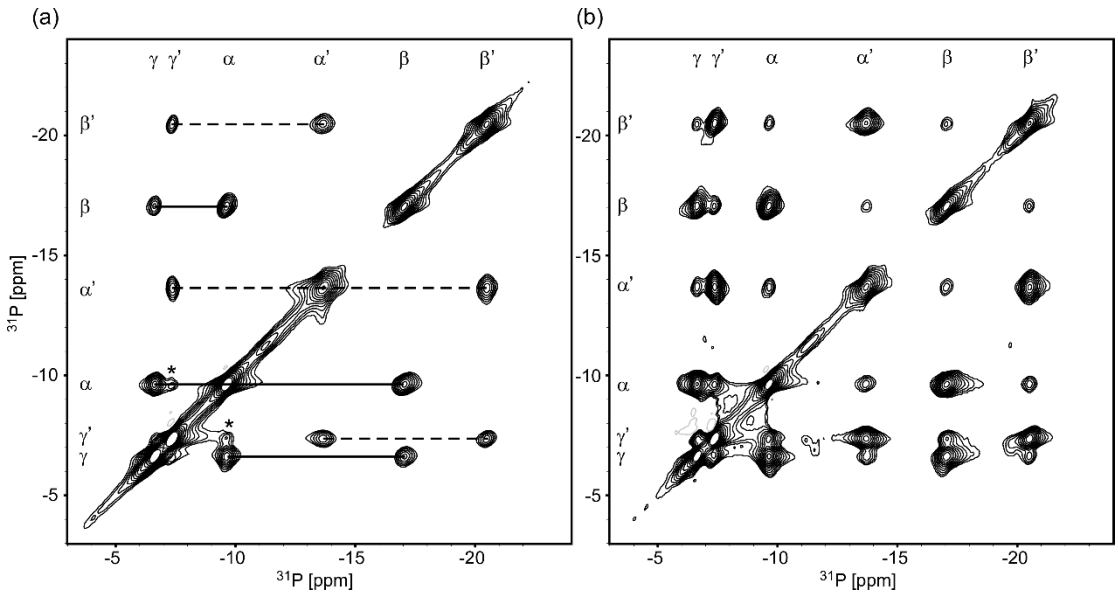

Figure 2. (a) 2D ^{31}P-^{31}P DARR of LiATP acquired with a short mixing time of 15 ms. The lines indicate correlations between adjacent phosphate groups, solid lines correlating signals within phosphates of one ATP molecule (α, β, γ), and the dashed lines for the second ATP molecule (α', β', γ'). The asterisks indicate P_{α}-$P_{\gamma'}$ correlations between the two ATP molecules. (b) 2D ^{31}P-^{31}P DARR of LiATP acquired with a mixing time of 100 ms. Many correlations between the two ATP molecules can be observed.

Following the DARR15 and CPMAS spectra, we could assign all ^{31}P signals and fit their CSA values, all of which are given in Table 1.

Table 1. Chemical shifts, CSA and asymmetry values for ^{31}P in LiATP:

^{31}P	P_{α}	P_{β}	P_{γ}	$P_{\alpha'}$	$P_{\beta'}$	$P_{\gamma'}$
δ_{iso} [ppm]	-9.6	-17.0	-6.6	-13.7	-20.5	-7.4
δ_{aniso} [ppm]	-106.3	-121.7	-117.0	-125.0	-121.3	-110.8
η	0.72	0.49	0.57	0.54	0.43	0.72

In order to estimate the organization of the dimer, more inter-molecular correlations should be obtained, and we performed another ^{31}P-^{31}P DARR experiment using a longer mixing time of 100 ms, allowing longer-range transfers, as shown in **Figure 2b**. From a qualitative analysis of the spectrum we can estimate the relative proximities of the phosphate groups from different molecules. The P_{α}-$P_{\gamma'}$ and P_{γ}-$P_{\gamma'}$ crosspeaks are the strongest of the inter-molecular correlations, and the fact that the P_{α}-$P_{\gamma'}$ are also strongly observed in DARR15 indicates the juxtaposition of these two phosphate groups. Clearly the weakest signals are those connecting P_{α}-$P_{\alpha'}$, P_{β}-$P_{\beta'}$ P_{α}-$P_{\beta'}$ and $P_{\alpha'}$-P_{β}. Correlations with intermediate strength are observed for P_{β}-$P_{\gamma'}$. Since in the CP spectrum the signal intensities for $P_{\alpha'}$, P_{β} and $P_{\beta'}$ are about half of the signals

of P_α, P_γ and $P_{\gamma'}$, we also deconvoluted the 2D spectrum (using the software DMFIT[37]), and normalized with respect to the 1D spectral intensities. Similar trends of the cross-peak intensities remain thus strengthening the conclusion that P_α and P_γ of one molecule are close to $P_{\gamma'}$ of a second molecule in the unit cell.

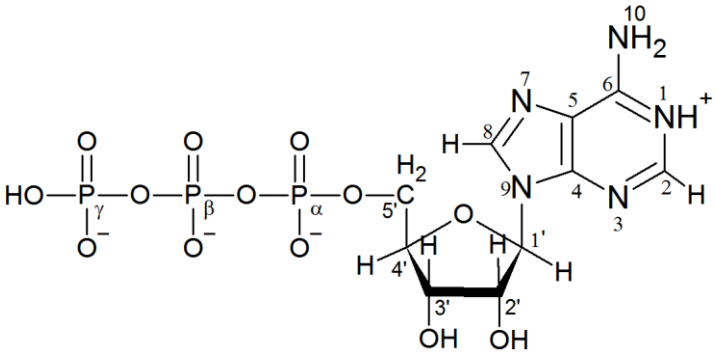

Scheme 1 Adenosine triphosphate. Amine base atoms are labeled 1-10, the ribose carbons are labeled 1'-5' and the phosphate atoms are labeled α, β, γ. The protonation scheme corresponds to an ATP molecule produced at a pH of ~3.

In order to observe the effect of lithium on ^{31}P shifts upon replacement of sodium in the complex, we compared the ^{31}P spectra of LiATP with that of a recrystallized disodium ATP trihydrate sample, prepared in a similar manner, and with existing prior data. An overlay of the ^{31}P CPMAS spectra is shown in **Figure 3**. Clear shifts are observed for all signals ($P_{\alpha'}$ is only slightly shifted). The 2D ^{31}P-^{31}P DARR15 correlation experiment of recrystallized NaATP, appearing in Fig. S1 of the SI, further shows that the resonances of the γ phosphates are reversed in LiATP, as also can be deduced from comparison to other studies of sodium ATP trihydrate[21]. Unlike in solution, where the addition of LiCl to sodium ATP resulted in a shift of all phosphates to higher values, despite the existence of some dihydrate crystals in our data, the change in the ^{13}P chemical shift is distinct, and we observe that P_α and $P_{\gamma'}$ shift to lower chemical shift values while the rest of the phosphates shift to higher chemical shift values. The largest shift observed is for P_β (+1.4 ppm) followed by $P_{\beta'}$ (+0.9 ppm) and P_α (-0.7 ppm). We will show later that these large shifts are in agreement with our observations that lithium binds to those phosphate groups. P_γ and $P_{\gamma'}$ chemical shift changes are close to that of P_α (~0.6 ppm), and they are shifted to opposite directions. The smallest change in chemical shift is observed for $P_{\alpha'}$.

The different trends in the chemical shift changes (both upfield and downfield) may imply on both the differences in complexation *i.e.* sodium vs. lithium, several sites vs. possibly a single metal site, changes in hydrogen bonding patterns, and on a change in the triphosphate chain conformation.

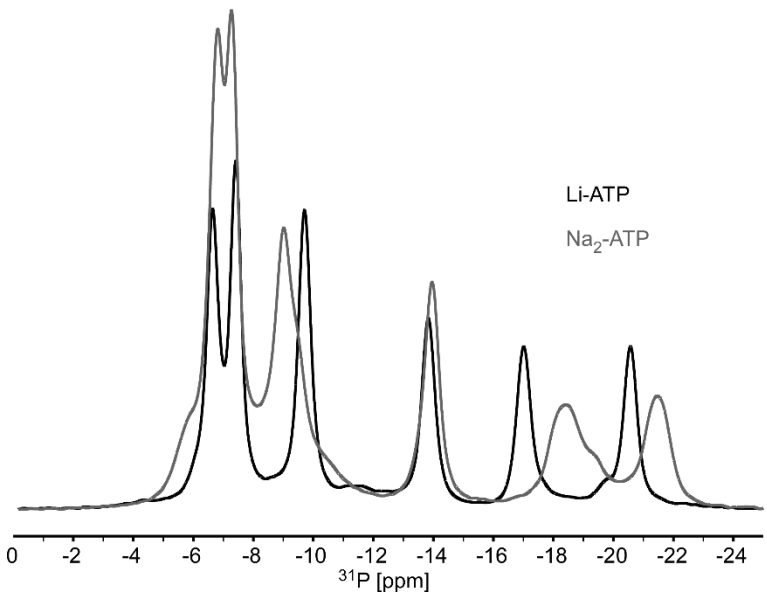

Figure 3. An overlay of the 1D ^{31}P CPMAS spectra of LiATP trihydrate (black) and NaATP trihydrate (gray). Only the center bands are shown. The order of P_{γ} and $P_{\gamma'}$ (the two peaks at ~ -7 ppm) is reversed in LiATP. Small contributions of the dihydrate form of NaATP can be observed as small shoulders in the spectrum of $P_{\gamma'}$ and P_{β}, presumably resulting from slight over-drying. Both spectra were acquired on a 9.4T spectrometer. LiATP assignment from left to right: P_{γ}, $P_{\gamma'}$, P_{α}, $P_{\alpha'}$, P_{β}, $P_{\beta'}$.

Direct observation of Lithium binding to ATP:

Direct detection of the ^{7}Li signal yielded a single (center-band) peak with a chemical shift of -0.12 ppm and a nuclear quadrupolar coupling constant of 50 kHz (determined by fitting the side band pattern of a slow spinning experiment). In order to examine the coordination of lithium to the different phosphate groups, we performed two lithium-phosphorous heteronuclear correlation experiments. A 2D transferred echo double resonance (TEDOR[38]) experiment to observe correlations, and possibly resolve different lithium sites, and a rotational echo double resonance (REDOR[39]) experiment in order to better quantify inter-nuclear ^{31}P-^{7}Li distances in the complex. Both experiments have been performed following our previous optimization schemes for ^{7}Li, applied to a complex of lithium, glycine and water (LiGlyW).[40]

A ^{7}Li-^{31}P TEDOR spectrum is presented in **Figure 4**. ^{7}Li correlations were observed with all phosphate groups save for $P_{\alpha'}$, which was below the noise level. Only a single lithium site is resolved, thus most probably we observe a single lithium site in the unit cell. Although the chemical shift dispersion of lithium is very small, such an experiment would have probably revealed differences between sites bound to different phosphates.

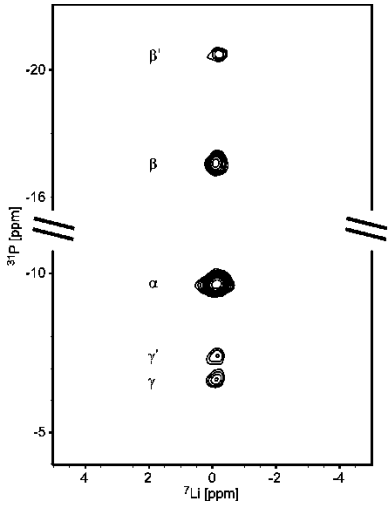

Figure 4. 2D $\{^{31}P\}^{7}Li$ TEDOR of $\{23\%-^{7}Li\}$-LiATP. The spectrum was acquired with a preparation mixing time of 714 μs (10 rotor periods) and a reconversion time of 1286 μs (18 rotor periods). The recoupling π pulses were applied on ^{31}P at both mixing times with the exception of a single echo pulse on ^{7}Li. Crosspeaks can be observed between Li at -0.15 ± 0.05 ppm and the phosphate atoms of both ATP molecules in the unit cell. No crosspeak with $P_{\alpha'}$ was detectable. All experimental details are given in the SI. Irradiating both ^{31}P and ^{7}Li, which have very close Larmor frequencies, was enabled by the use of a frequency splitter ('REDOR-BOX', ©NMR service GmbH).

An initial assessment of the proximity of lithium to the different ^{31}P atoms can be obtained from the analysis of the cross-peak intensities, as shown in **Table 2**. Since ^{31}P intensities are not similar (**Figure 1**) we normalized the TEDOR crosspeaks intensities according to the $^{1}H-^{31}P$ CP intensities in order to obtain a more accurate estimation of the transfer efficiency of each phosphate group to lithium. Lithium has the strongest correlation to P_{β} followed by P_{α} and $P_{\beta'}$, results that are in agreement with the ^{7}Li-induced ^{31}P shifts observed above. P_{γ} and $P_{\gamma'}$ show the weakest signals, and $P_{\alpha'}$ is barely detected above the noise level. Lithium strongly correlating to three phosphates is in agreement with the preferred tetrahedral coordination for lithium, as we observed in LiGlyW[40] (correlations to carboxyl groups), assuming that the fourth ligand is a water molecule, a base nitrogen, or from the ribose.

Table 2.^{31}P CP relative intensities and $\{^{31}P\}^{7}Li$ TEDOR normalized crosspeak intensities in LiATP. All intensities were normalized according to $P_{\gamma'}$.

	P_{α}	P_{β}	P_{γ}	$P_{\alpha'}$	$P_{\beta'}$	$P_{\gamma'}$
$^{1}H-^{31}P$ CP	1.10	2.64	1.19	2.66	2.69	1
TEDOR	3.85	5.05	1.45	-	3.15	1

In order to better quantify the coordination of lithium, we performed CPMAS-filtered $\{^{7}Li\}^{31}P$ REDOR experiments in order to extract $^{7}Li-^{31}P$ distances. All REDOR curves are presented in **Figure 5**Error! Reference source not found.. It can be seen that the three phosphate groups P_{β}, P_{α} and $P_{\beta'}$ show the strongest recoupling, and have a

similar initial slope indicating a comparable inter-nuclear distance. The other three phosphate groups also show a comparable recoupling curve however they are clearly more distant from the lithium ion.

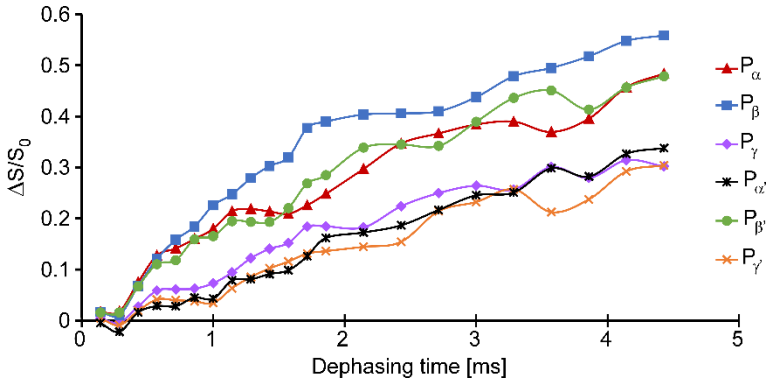

Figure 5. Experimental CP-filtered $\{^{7}Li\}^{31}P$ REDOR dipolar recoupling curves for the six non-equivalent ^{31}P sites in $\{23\%-^{7}Li\}$-LiATP. In the REDOR sequence all dephasing pulses were applied to the ^{7}Li channel due to the relatively large CSA of the ^{31}P spins. P_{α}, P_{β} and $P_{\beta'}$ are closest to the lithium center. The REDOR fraction $\Delta S/S_0$ is given by $(S_0-S)/S_0$ where S_0 is a reference signal obtained from the intensity of the ^{31}P spectrum obtained without the pulses on lithium, and S is the signal with all pulses.

In order to quantify the inter-nuclear $^{31}P-^{7}Li$ distances we first examined the effect of various multi-spin systems on the signals, and assumed a single lithium site, since we can only resolve a single lithium signal, even when attempting to separate the sites with a triple-quantum/single quantum ^{7}Li correlation experiment, as done before for lithium in the enzyme Inositol monophosphatase[41]. Simulations of a LiP_n spin system with n=1-3 were performed taking into account the nuclear quadrupolar coupling constant C_Q of lithium, and CSA values of the phosphates, obtained from our experimental data. $^{31}P-^{31}P$ homonuclear dipolar couplings, and Euler angles relating the CSA and dipolar tensors were extracted from the structure of NaATP[21]. The simulations (SI, **Figure S2**) showed that the initial rise of the REDOR curve (from which the inter-nuclear distance can be measured) was unaffected by the spin system size or by the Euler angles of the interaction tensors. Small oscillations were observed at longer dephasing times and do not affect the analysis of the initial rise. Thus we concluded that two spin system simulations were sufficient.

The experimental data for the six ^{31}P species shown in **Figure 5** were then deconvoluted (using the software DMFIT[37]) and fit individually to simulations at a range of $^{31}P-^{7}Li$ distances using a single spin pair. **Figure 6** shows the results for the closest ^{31}P spins, P_{α}, P_{β}, and $P_{\beta'}$. All curves are in agreement with a distance of ~3.0Å. **Figure 7** shows the results for $P_{\alpha'}$, P_{γ}, and $P_{\gamma'}$, and they report on distances of 3.6-4.2 Å. Reported metal-phosphorus distances in ATP complexes are ~3.4-3.8Å in sodium ATP[22–24] and ~3.1-3.3Å in magnesium ATP[29,30]. Thus, the distances are in a better

agreement with the MgATP complex. The current results of oxygen-mediated ^{7}Li-^{31}P are also in agreement with prior observations of oxygen-mediated ^{7}Li-^{31}C distances including our studies of the LiGlyW complex,[40,42] and of lithium binding in the enzyme inositol monophosphatase.[41] Thus they represent typical Li-O-X coordination.

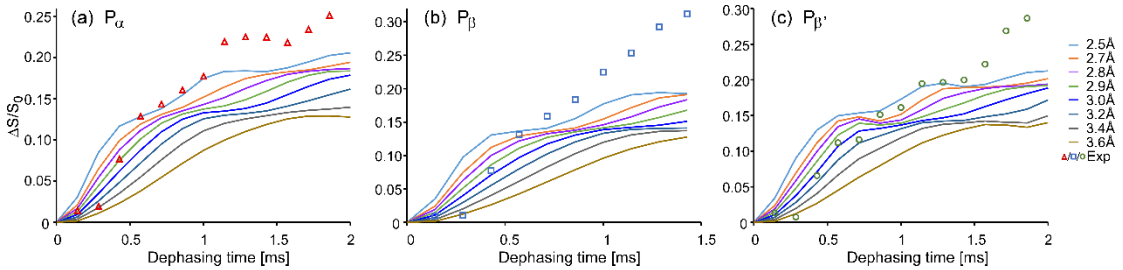

Figure 6. Comparison of experimental CP-filtered, ^{31}P-detected REDOR data points of the phosphate signals (a) P_{α}, (b) P_{β} and (c) $P_{\beta'}$ from {23%-^{7}Li}-LiATP with simulations of single Li–P spin pairs at distances of 2.5-3.6 Å. The simulations were multiplied by 0.2338 in order to account for the labeling pattern and the natural ^{7}Li percentage. The best fit is for a distance of ~3.0Å (a dipolar interaction D of 700 Hz). The deviation of the experimental points beyond ~1 ms occurs due to the existence of remote ^{7}Li labeled sites.

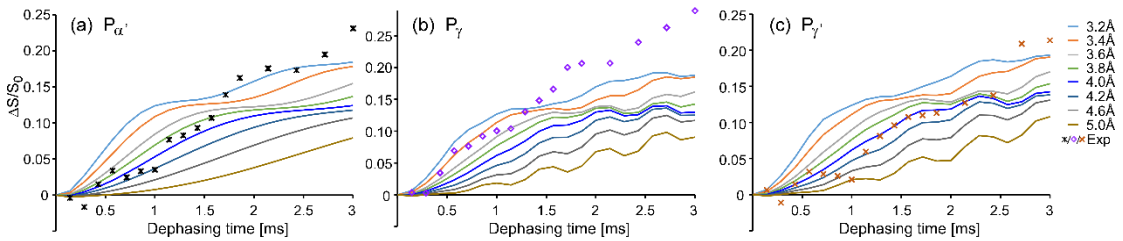

Figure 7. Comparison of experimental CP-filtered, ^{31}P-detected REDOR data points ($\Delta S/S_0$) of the phosphorous signals (a) $P_{\alpha'}$, (b) P_{γ} and (c) $P_{\gamma'}$ from {23%-^{7}Li}-LiATP with simulations of single Li–P spin pairs at distances of 3.2-5.0 Å. Best fit for $P_{\alpha'}$ is 4.0 ± 0.2Å (D = 300 Hz), for P_{γ} is 3.4 ± 0.2Å (D = 480 Hz) and for $P_{\gamma'}$ is 3.8 ± 0.4Å (D = 350 Hz). The oscillatory nature of the curves for $P_{\gamma/\gamma'}$ is probably caused by off resonance effects ($P_{\alpha'}$ is on resonance and $P_{\gamma/\gamma'}$ has an offset of 6-7 ppm). The deviation of the experimental points beyond ~1.5 ms occurs due to the existence of remote ^{7}Li labeled sites.

While the data above are sufficiently reliable to provide clear evidence on the proximity of lithium to the various phosphate moieties, several errors may marginally affect the quantification of our data. As discussed above, the initial rise is the most important region for a successful fit, however, the number of data points in this region for the shorter distances is small due to (i) the hardware limitation of using of a moderate spinning speed of 14 kHz (hence longer times between the detection points); (ii) experimental deviations for data points taken when a full XY4 or XY8 refocusing

cycle could not be used, evident for the second data point in Figure 6. Yet, these do not affect the conclusions -

From ^{31}P and ^{7}Li shifts, from ^{31}P-^{7}Li correlation NMR experiments, and from ^{31}P-^{7}Li distance measurement experiments, clearly a single lithium site is coordinated to P_{α}, P_{β} and $P_{\beta'}$, with inter-nuclear ^{31}P-^{7}Li distances of ~ 3Å.

^{1}H NMR and the spatial organization of LiATP

In order to further characterize the triphosphate chain and the coordination of lithium in the LiATP complex, we performed 2D heteronuclear correlation experiments involving protons. Both ^{1}H–^{31}P *w*PMLG–HETCOR spectra and fast MAS ^{1}H-detected $\{^{1}H\}^{31}P$-^{1}H spectra, shown in **Figure 8**, show signals of acidic protons and of other protons belonging to the adenine base and the ribose. Identification of the signals is in part supported by the solution NMR spectrum shown and assigned in the SI (**Figure S3**). Two strong signals, resonating at 11.6 ppm and 15.3 ppm are missing from the solution spectrum, and exist in the MAS spectrum. A third, weaker signal appears only in the fast MAS spectrum acquired at 62 kHz. Those signals belong to exchangeable acidic protons. Their assignment is based on their relative intensities at different mixing times; the signal resonating at 11.6 ppm shows strong correlations to the gamma phosphates, and has very fast build-up rates (see SI, **Figure S4**). It also shows correlations to P_{α} and $P_{\alpha'}$ although with a lower intensity. This signal therefore corresponds to the acidic P_{γ} phosphate groups. Indeed such shifts are typical of hydrogen bonded protonated phosphates[43]. The correlations to the alpha phosphates are indicative of the spatial organization of the tri-phosphate moiety locating P_{γ} of one ATP molecule between $P_{\alpha'}$ and $P_{\gamma'}$ of a second ATP molecule. In our preparation of the LiATP, the pH value was approximately 2-3, and following previous studies[44–47] indicating that one hydroxyl group of the gamma phosphate has a pKa of ~1-2 and the second group has a pKa of ~6-7, we conclude that only one of the gamma phosphates is protonated. Thus, the other low-field signal that shows strong correlations to primarily P_{γ} and $P_{\gamma'}$ at 15.3 ppm, albeit with a smaller intensity, does not belong to a phosphate group. Unlike the signal at 11.6 ppm, the correlation to P_{α} is much weaker and correlations to both $P_{\beta/\beta'}$ phosphates appear as well.

Since the pKa of N1 is ~4-5[44,45], it is protonated in our preparation. Imino NH protons involved in Watson-Crick hydrogen bonding resonate at 12-14 ppm, and in isocytosine and guanosine-derivatives for example,[48,49] they have chemical shifts of 13-15 ppm. Thus the peak at 15.3 ppm can be attributed to the imino proton attached to N1 and is probably subjected to strong hydrogen bonding. The strong correlations to $P_{\gamma/\gamma'}$ suggest a bending of the base towards the edge of the triphosphate of the second ATP molecule. Approximate similar intensities of crosspeaks to $P_{\alpha/\alpha'}$, and to $P_{\beta/\beta'}$

correspond to the location of the ring mid-way between its own P_α (or $P_{\alpha'}$) and the $P_{\beta'}$ (or P_β) of the second ATP molecule.

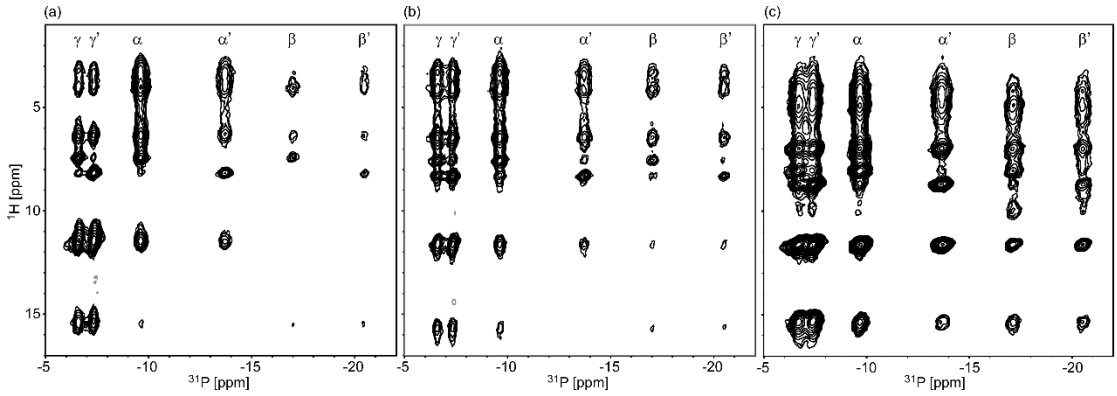

Figure 8. ^{1}H-^{31}P $wPMLG_{m\bar{m}}^{x\bar{x}}$ [50,51] HETCOR spectra of LiATP acquired at a spinning speed of 11.5 kHz (at 0°C) and CP contact times of (a) 1 ms and (b) 3 ms. The ^{1}H axis is scaled. (c) ^{1}H-detected $\{^1H\}^{31}P$-^{1}H HETCOR MAS spectrum of LiATP acquired at a spinning speed of 62 kHz (at -30°C) with a $^{31}P \rightarrow {}^1H$ CP contact time of 2.75 ms. The spectrum was flipped in order to align the axes of all spectra in the Figure. The final ^{1}H chemical shifts were determined according to fast MAS ^{1}H-detected experiment (c). A full list of experimental parameters appears in the SI.

Additional proton correlation experiments have been performed with lithium. A *w*PMLG-HETCOR experiment acquired with a short mixing time (**Figure 9a**) does not reveal contacts of lithium with the acidic protons, further strengthening our conclusion that lithium is not in proximity to P_γ. Such correlations only appear at a longer mixing time (**Figure 9b,** fast MAS ^{1}H-detected $\{^1H\}^7Li$-^{1}H HETCOR). The projection of the ^{1}H spectrum reveals a broad hump underneath the spectrum, which was not apparent in the ^{31}P-^{1}H spectrum. Most probably this signal correspond to a water molecule (or several) that coordinates lithium, completing its fourth coordination. Correlations with some of the ribose signals appear at 4-7 ppm, which cannot be faithfully assigned at this stage, however are in line with the fact that lithium coordinates P_α and is thus in proximity to those hydrogens.

Potential assignments of the ^{1}H signals, based on ^{1}H-X correlations, on ^{1}H-^{31}P build-up curves, and on the ^{1}H solution NMR spectrum of LiATP appear in the SI.

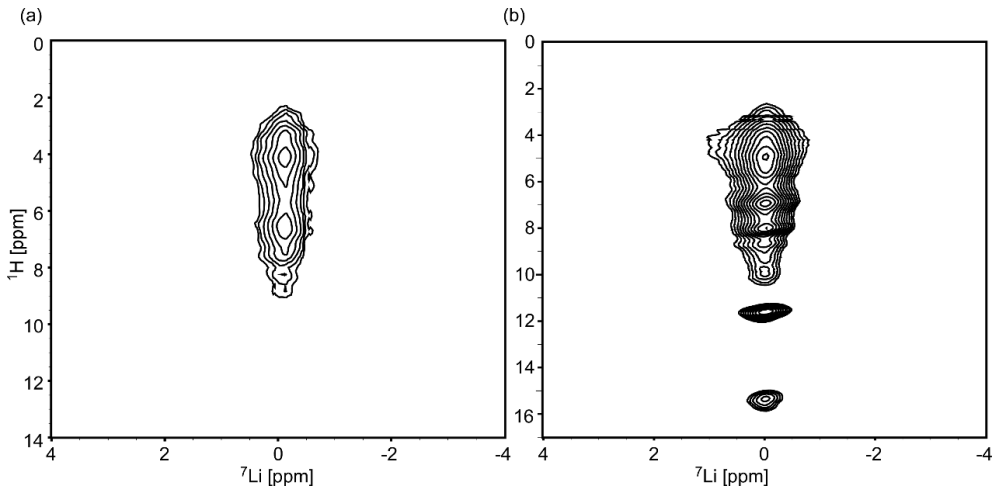

Figure 9. (a) ^{1}H-^{7}Li $wPMLG_{m\bar{m}}^{x\bar{x}}$ HETCOR spectrum of {23%-^{7}Li}-LiATP acquired at a spinning speed of 11.5 kHz (at -20°C), and a CP contact time of 0.5 ms. The ^{1}H axis is scaled. (b) Fast MAS (62 kHz at -30°C) {^{1}H}^{7}Li-^{1}H HETCOR of {NA-^{7}Li}-LiATP acquired with a CP contact time of 1.7 ms. The spectrum was flipped in order to align the axes of all spectra in the Figure. The final ^{1}H chemical shifts were determined according to the fast MAS ^{1}H-detected experiment. A full list of experimental parameters appears in the SI.

Residual sodium in LiATP

The LiATP complex was prepared from mixing excess LiCl with commercial disodium ATP trihydrate, in the molar ratio Li:Na of 10:1. Therefore, sodium may remain as a complex of the form NaLiATP, or as a residual with no specific role in the complex. In the trihydrate form of NaATP there are four chemically inequivalent sites according to X-ray crystallography[23], as well as multiple-quantum MAS NMR[28] (also observed by us, see SI, **Figure S5**). An overlay of 1D MAS ^{23}Na spectra of LiATP and of recrystallized NaATP are shown in **Figure 10**. Clearly some of the sodium signal disappears in the 1D ^{23}Na spectrum of LiATP, however, two signals (at least) remain; a narrow peak and a broadened signal. MQMAS spectra revealed three sites (**Figure S5**) and a three-site-fit for the 1D experiment generated C_Q values of approximately 0.85, 2.3 MHz and 0.95 MHz, respectively, where the third site has a low occupancy in comparison to the other two.

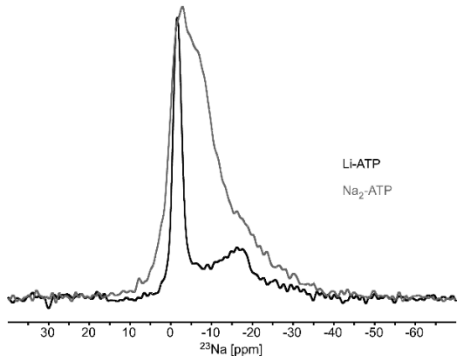

Figure 10. Overly of 1D ^{23}Na spectra of LiATP (black) and NaATP (gray). MQMAS spectra of both samples appear in the SI, Fig. S5.

In order to further characterize these sodium sites, we performed $\{^{23}Na\}^{31}P$ and $\{^{23}Na\}^{7}Li$ PM-RESPDOR[52,53] distance measurement experiments. A $\{^{23}Na\}^{7}Li$ PM-RESPDOR recoupling curve is shown in **Figure 11**. We observe a clear recoupling of the lithium signal that is consistent with an inter-nuclear distance of 4.3Å, and the recoupling approaches the theoretical limit for a spin-3/2 of $\Delta S/S_0$=0.75. Therefore, it is most likely that at least one site in every ATP molecule can be attributed to sodium in close proximity to lithium. Since MQMAS suggests that at least two sodium sites exist in every ATP dimer, we can assume that both are in similar proximity to lithium and a simulation with two sodium sites shows even a better fit (at longer times) than a single spin-pair, and the estimated distance then increases up to ~5Å. In both cases, every ATP molecule must have a persistent high affinity sodium site.
Furthermore, looking at one point in a $\{^{23}Na\}^{31}P$ PM-RESPDOR experiment (**Figure 11b**) reveals that the sodium atom coordinates to P_γ, $P_{\gamma'}$, and to a lower extent, to P_α. The complete recoupling curves are shown in the SI, **Figure S6**. Assuming a decay from a single sodium spin, fitting the ^{31}P signal of P_γ, is consistent with a distance of ~3 Å, which is too short when comparing to the reported Na-P distances in Na_2ATP .[22–24] A fit involving two sodium sites yields more plausible distances of ~3.3-3.4 Å.

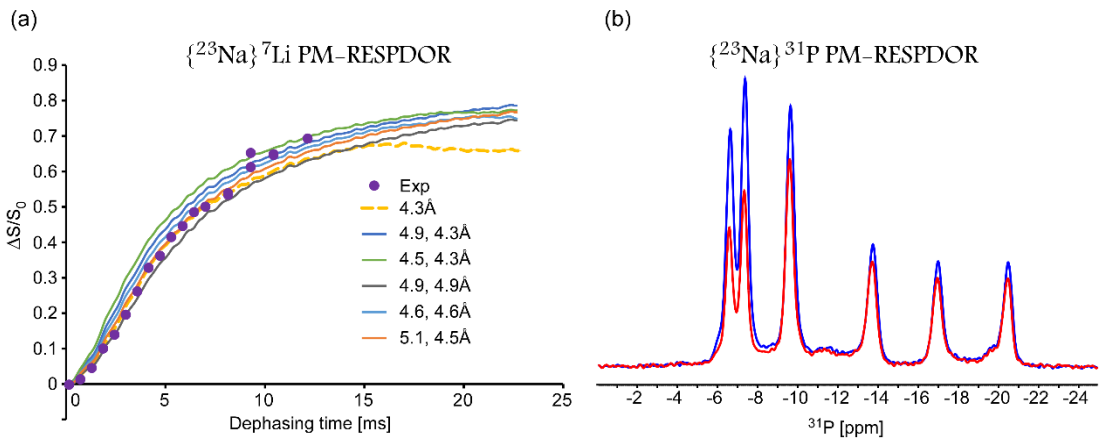

Figure 11. (a) PM-RESPDOR $\{^{23}Na\}^{7}Li$ recoupling curve of LiATP. A fit to an isolated pair yields a lithium-sodium distance of 4.3Å (dash line, D = 150 Hz). The experimental points $\Delta S/S_0$ are shown as circles. SIMPSON simulated curves for two sodium sites at various distances up to 5.1Å are shown and the experimental data are in good agreement with D = 90, 130 Hz (orange line, 4.5Å, 5.1Å). (b) A single $\Delta S/S_0$ point on the PM-RESPDOR $\{^{23}Na\}^{31}P$ recoupling curve, acquired at a mixing time of 1.3 ms, showing the S_0 reference signal (blue) and the decay signal S (red). From left to right in the spectrum of LiATP, P_γ and $P_{\gamma'}$ have the most pronounced initial decay, followed by P_α. A much slower decay is observed for the other phosphates.

Another way to directly determine if the additional sodium sites are part of the structure, and to characterize their environment, is to perform sodium-detected REDOR experiments. We therefore implemented $\{^{31}P\}^{23}Na$ REDOR and $\{^{7}Li\}^{23}Na$ REDOR experiments. We observe that in both experiments (**Figure 12** and **Figure S7**) all sodium sites decay with an approximately equal rate. Thus, there must be at least two inequivalent sodium sites in the sample (and a possible third site with ~ 30-35% occupancy). The $\{^{7}Li\}^{23}Na$ REDOR experimental results in **Figure 12** show that sodium recoupling reaches ~0.5 (with 24% dilution of ^{7}Li) rather than the theoretical 0.24, suggesting that every sodium atom is in contact with two lithium sites. A two spin system simulation shows a reasonable fit to a distance of 5.5Å. This is in agreement with the inverse $\{^{23}Na\}^{7}Li$ PM-RESPDOR measurements.

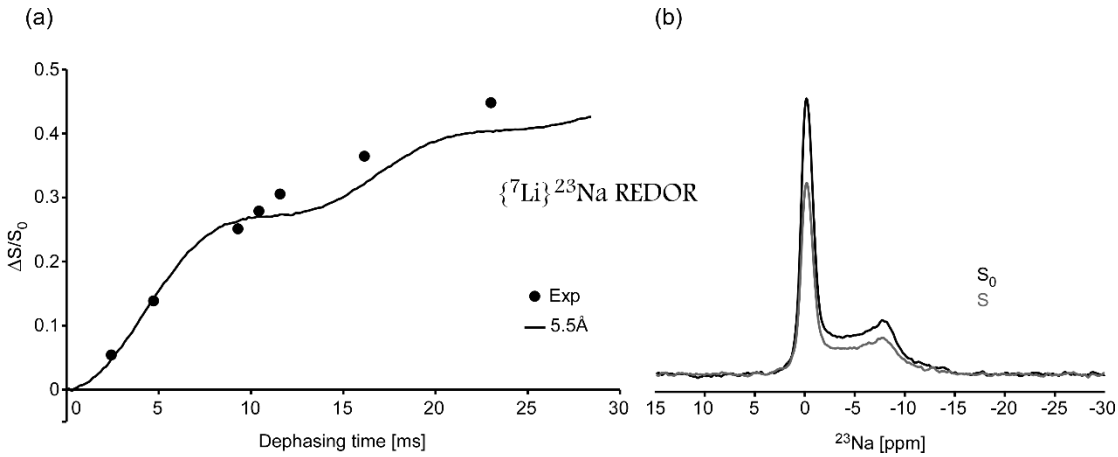

Figure 12. (a) $\{^{7}Li\}^{23}Na$ REDOR recoupling curve in LiATP. Data points represent the integral of the entire sodium signal. A SIMPSON simulated curve for a Li-Na distance of 5.5Å (D = 70 Hz) is shown. (b) A single $\Delta S/S_0$ point acquired at a mixing times of 11.57 ms showing the S_0 reference signal (black) and the decay signal S (gray). It can be seen that the dephasing seems to be uniform.

Proposed schematic model for lithium binding to ATP

Based on the results of this work we are able to propose the schematic model for lithium binding in the lithium ATP complex shown in **Figure 13**. In the solid phase, LiATP is a dimer, similarly to MgATP and NaATP. The arrangement is such that P_γ of one molecule is located between $P_{\alpha'}$ and $P_{\gamma'}$ of a second ATP molecule, with $P_{\beta'}$ located at an angle to both. Lithium is coordinated to the three phosphates P_α, P_β and $P_{\beta'}$ at a distance of ~3Å, and a forth ligand is presumably a water molecule. The adenine ring is somewhat tilted positioning its imino proton N_1H^+ towards the gamma phosphate of a second ATP molecule.

Every such complex also has at least two sodium cations despite the fact that lithium was used in excess. These sodium ions are located at a distance of 4.3 – 5.5 Å from two lithium sites (both at equivalent positions, probably belonging to two different

unit cells), and are coordinated to the phosphates P_γ and $P_{\gamma'}$, with P_α the next closest phosphate.

Despite the fact that the model is not complete in the sense that we cannot determine atomic coordinates at this stage, it demonstrates well the coordination of lithium, the strong affinity of the sodium sites, and the overall organization of the two ATP molecules.

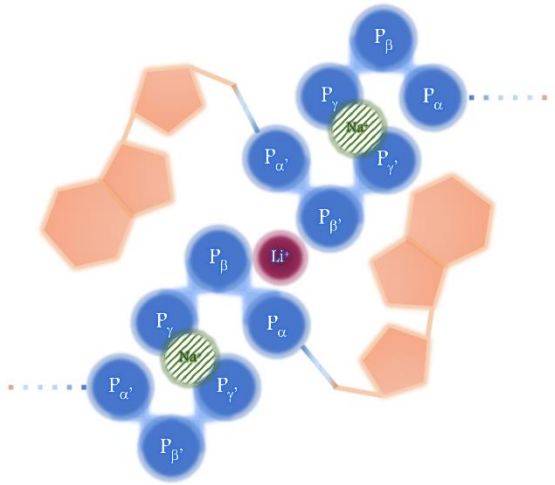

Figure 13. A schematic model for lithium binding to two ATP molecules via three phosphate groups.

A more elaborate atomic-resolution model requires additional experiments and probably a full NMR crystallography approach.

Conclusions

Lithium is one of the most prominent drugs for various mental illnesses, mainly bipolar disorder. Lithium binds many enzymes as well as ATP, "the chemical energy of life". In this paper we characterize the complex of lithium with ATP using a multi-nuclear MAS solid-state NMR approach. The experiments included simple one-dimensional spectra, two-dimensional correlation experiments involving lithium, phosphates and sodium, ^{1}H correlation experiments, and explicit distance measurements.

Based on all the accumulated data we can define the lithium coordination and identify the existence of structural sodium ions, bound to the complex in high affinity. To the best of our knowledge, an experimental model based on direct observation of lithium does not exist, while other models in solution suggest binding to gamma phosphates. Here we show a model of binding for the LiATP complex, in which lithium coordinates to the three phosphate groups P_α, P_β and $P_{\beta'}$ with equivalent distances, and to a water molecule. Li-P distances are similar to those in MgATP[17], to Li-C in a lithium-glycine-water complex[40], and similar to Li-C in the enzyme inositol monophosphates, the putative target of lithium therapy[41]. This is a result that stems

from the fact that Li^+ and Mg^{2+} have a similar ionic radii.[54] The methods we present here are suitable for characterization of Metal-bound ATP molecules, even when a mixture of cations exist, a state depicting more biologically relevant situations.

Experimental Section

Preparation of a lithium-ATP-water complex

LiATP was prepared by a small modification of the diffusion procedure described by Potrzebowski et al.[21] A 20:1 mole ratio of LiCl and $Na_2ATP{\cdot}3H_2O$ (purchased from Fisher Bioreagents) was dissolved in purified water and isopropyl alcohol (IPA) was added to a ratio of 1:2.5 v/v Water:IPA. The flask containing the solution was then placed in a vessel filled with pure IPA and was left overnight at room temperature to crystalize. The solid material was filtered out, washed with IPA, and dried on a Büchner funnel. In this manner three ATP sample types were prepared that differ in the amount of lithium-7: (i) {23-24%-^{7}Li}-LiATP: a mixture of ~25 w/w% natural abundance LiCl and ~75 w/w% ^{6}LiCl; (ii) {36%-Li}-LiATP; (iii) {92%-Li}-LiATP termed NA LiATP – this is the natural abundance sample.

A trihydrate sodium-ATP-water complex was recrystallized following the diffusion procedure described by Potrzebowski et al.[21] Prior to recrystallization the sample showed broad ^{31}P lines indicating lack of a clear crystalline state, or a mixture of hydration states.

NMR Instrumentation and Referencing

The majority of solid state NMR experiments were performed on a Bruker Avance-III spectrometer operating at a magnetic field of 14.1T, corresponding to Larmor frequencies of 600.2 MHz for ^{1}H, 242.9 MHz for ^{31}P, 233.2 MHz for ^{7}Li, and 158.7 MHz for ^{23}Na. Experiments were performed using a wide-bore 4mm probe operating in double resonance ^{1}H-^{31}P and ^{1}H-^{7}Li modes, in a ^{1}H-^{31}P-^{7}Li mode using a REDOR BOX (©NMR service GmbH) frequency splitter, and in triple-resonance ^{1}H-^{31}P-^{23}Na and ^{1}H-^{7}Li-^{23}Na modes. Additional experiments were carried out using a fast-spinning 1.3mm probe operating in double-resonance ^{1}H-^{31}P or ^{1}H-^{7}Li modes.
Some measurements were performed on a Bruker Avance-III spectrometer operating at a magnetic field of 9.4T, corresponding to Larmor frequencies of 400.2 MHz for ^{1}H, 162.0 MHz for ^{31}P, and 105.9 MHz for ^{23}Na using a wide-bore 4mm probe operating in ^{1}H-^{31}P and ^{1}H-^{23}Na double-resonance modes.

Spectra were externally referenced to adamantane at 1.8 ppm for ^{1}H, to O-phospho-L-Serine at 0.3 ppm for ^{31}P, to 1M LiCl solution at 0 ppm for ^{7}Li, and to 0.1M NaCl solution at 0.29 ppm for ^{23}Na (calibrated by secondary external referencing with adamantane). The experiments were performed at different temperatures and the reported values are the temperatures set at the entrance to the probe, which is lower than the actual sample temperature due to frictional heating during sample spinning. Detailed experimental parameters are given in the captions and in the supplementary information.

Simulations and fitting of distance measurement experiments

All simulations were performed using the software SIMPSON[55]. ^{31}P-detected REDOR simulations were carried out for an isolated ^{7}Li–^{31}P spin pair, and for three (P_2-Li) and four (P_3-Li) spin systems taking into account isotropic shifts, CSA, C_Q and all homonuclear and heteronuclear interactions. The carrier frequency was set on-resonance for lithium and to the $P_{\alpha'}$ atom for phosphorus. The values of C_Q (50 kHz) and of the ^{31}P CSA were set according to the experimentally fitted lineshapes in a {36%-Li}-LiATP sample. ^{31}P-^{31}P homonuclear dipolar interactions, and Euler angles for the CSA tensors and the homonuclear dipolar tensors for the first ATP molecule were all adapted from sodium ATP studies.[21] Euler angles for CSA tensors for the second ATP molecule (two ATP molecules exist in the unit cell) were modified to create a semi mirror image. For the analysis of LiATP data, simulations were performed for different heteronuclear dipolar coupling constants. ^{31}P and ^{7}Li detected PM-RESPDOR and ^{23}Na detected REDOR simulations were carried out for two (P-Na or Li-Na) or three (P-Na_2 or Li-Na_2) spin systems. Parameters for lithium and phosphorous were similar to the above REDOR simulations. For sodium C_Q values of 0.76 MHz and 2.0 MHz were used.

Acknowledgement

This research was funded by support from the US-Israel Binational Science Foundation awarded to AG and Tatyana Polenova.

References

[1] W. Young, *Cell Transplant.* **2009**, *18*, 951–975.

[2] H. Eldar-Finkelman, *Trends Mol. Med.* **2002**, *8*, 126–132.

[3] J. A. Quiroz, T. D. Gould, H. K. Manji, *Mol. Interv.* **2004**, *4*, 259–272.

[4] R. S. El-Mallakh, *Clin. Neurosci. Res.* **2004**, *4*, 227–231.
[5] K. Burton, *Biochem. J.* **1959**, *71*, 388–395.
[6] L. Nanninga, *Biochim. Biophys. Acta* **1961**, *16*, 330–338.
[7] W. J. O'Sullivan, D. D. Perrin, *Biochemistry* **1964**, *3*, 18–26.
[8] M. S. Mohan, G. A. Rechnitz, *Arch. Biochem. Biophys.* **1974**, *162*, 194–199.
[9] R. Adolfsen, E. N. Moudrianakis, *J. Biol. Chem.* **1978**, *253*.
[10] J. Wilson, A. Chin, *Anal. Biochem.* **1991**, *19*, 16–19.
[11] M. M. Taqui Khan, A. E. Martell, **1962**, *66*, 10–15.
[12] E. O. Bishop, S. J. Kimber, D. Orchard, B. E. Smith, *BBA - Bioenerg.* **1981**, *635*, 63–72.
[13] R. Prigodich, P. Haake, *Inorg. Chem.* **1985**, 89–93.
[14] A. Abraha, D. E. M. Defreitas, M. Margarida, C. A. Castro, C. Geraldes, *J. Inorg. Biochem.* **1991**, *42*, 191–198.
[15] M. Cohn, T. R. Hughes, *J. Biol. Chem.* **1962**, *237*, 176–182.
[16] T.-D. Son, M. Roux, M. Ellenberger, *Nucleic Acids Res.* **1975**, *2*, 1101–1110.
[17] F. Ramirez, J. F. Marecek, *Biochim. Biophys. Acta* **1980**, *589*, 21–29.
[18] J. L. Bock, *J. Inorg. Biochem.* **1980**, *12*, 119–30.
[19] L. Amari, B. Layden, Q. F. Rong, C. Geraldes, D. M. de Freitas, *Anal. Biochem.* **1999**, *272*, 1–7.
[20] Y. Shindo, A. Naito, S. Tuzi, Y. Sugawara, *J. Mol. Struct.* **2002**, *603*, 389–397.
[21] M. J. Potrzebowski, J. Gajda, W. Ciesielski, I. M. Montesinos, *J. Magn. Reson.* **2006**, *179*, 173–181.
[22] O. Kennard, N. W. Isaacs, W. D. S. Motherwell, J. C. Coppola, D. L. Wampler, A. C. Larson, D. G. Watson, *Proc. R. Soc. A Math. Phys. Eng. Sci.* **1971**, *325*, 401–436.
[23] a. C. Larson, *Acta Crystallogr. Sect. B Struct. Crystallogr. Cryst. Chem.* **1978**, *34*, 3601–3604.
[24] Y. Sugawara, N. Kamiya, H. Iwasaki, T. Ito, Y. Satow, *J. Am. Chem. Soc.* **1991**, 5440–5445.
[25] S. Ding, C. McDowell, *Chem. Phys. Lett.* **2000**, 316–322.
[26] A. Wong, G. Wu, *J. Phys. Chem. A* **2003**, 579–586.
[27] C. V Grant, D. McElheny, V. Frydman, L. Frydman, *Magn. Reson. Chem.* **2006**, *44*, 366–74.
[28] M. Nausner, J. J. Brus, M. Haeubl, N. Mueller, W. Schoefberger, M. Häubl, N. Müller, *Inorganica Chim. Acta* **2009**, *362*, 1071–1077.
[29] R. Cini, M. C. Burla, A. Nunzi, G. P. Polidori, P. F. Zanazzi, *J. Chem. Soc. Dalt. Trans.* **1984**, 2467.
[30] G. Tamasi, F. Berrettini, M. B. Hursthouse, R. Cini, *open Crystallogr. J.* **2010**, *3*,

1–13.

[31] R. Cini, M. Sabat, M. Sundaralingam, M. C. Burla, A. Nunzi, G. Polidori, P. F. Zanazzi, *J Biomol Struct Dyn* **1983**, DOI 10.1080/07391102.1983.10507470.

[32] C. Grant, V. Frydman, L. Frydman, *J. Am. …* **2000**, 11743–11744.

[33] D. Mota de Freitas, M. M. C. A. Castro, C. F. G. C. Geraldes, *Acc Chem Res* **2006**, *39*, 283–291.

[34] K. T. Briggs, G. G. Giulian, G. Li, J. P. Y. Kao, J. P. Marino, *Biophys. J.* **2016**, *111*, 294–300.

[35] T. Dudev, C. Grauffel, C. Lim, *Sci. Rep.* **2017**, *7*, 1–10.

[36] K. Takegoshi, S. Nakamura, T. Terao, *Chem. Phys. Lett.* **2001**, *344*, 631–637.

[37] D. Massiot, F. Fayon, M. Capron, I. King, S. Le Calve, B. Alonso, J. O. Durand, B. Bujoli, Z. H. Gan, G. Hoatson, *Magn. Reson. Chem.* **2002**, *40*, 70–76.

[38] A. W. Hing, S. Vega, J. Schaefer, *J. Magn. Reson.* **1992**, *96*, 205–209.

[39] T. Gullion, J. Schaefer, *J. Magn. Reson.* **1989**, *81*, 196–200.

[40] A. Haimovich, A. Goldbourt, *J. Magn. Reson.* **2015**, *254*, 131–138.

[41] A. Haimovich, U. Eliav, A. Goldbourt, *J. Am. Chem. Soc.* **2012**, *134*, 5647–5651.

[42] U. Eliav, A. Haimovich, A. Goldbourt, *J. Chem. Phys.* **2016**, *144*, DOI 10.1063/1.4938415.

[43] X. Xue, M. Kanzaki, *J. Am. Ceram. Soc.* **2009**, *92*, 2803–2830.

[44] M. Matthies, G. Zundel, *J. Chem. Soc. Perkin Trans. 2* **1977**, 1824–1830.

[45] J. L. Oscarson, P. Wang, S. E. Gillespie, R. M. Izatt, G. D. Watt, C. D. Larsen, J. A. R. Renuncio, *J. Solution Chem.* **1995**, *24*, 171–200.

[46] R. N. Goldberg, Y. B. Tewari, *Biophys. Chem.* **1991**, *40*, 241–261.

[47] R. M. Smith, A. E. Martell, Y. Chen, *PURE Appl. Chem.* **1991**, *63*, 1015–1080.

[48] A. L. Webber, S. Masiero, S. Pieraccini, J. C. Burley, A. S. Tatton, D. Iuga, T. N. Pham, G. P. Spada, S. P. Brown, *J. Am. Chem. Soc.* **2011**, *133*, 19777–19795.

[49] M. Dračínský, P. Hodgkinson, *RSC Adv.* **2015**, *5*, 12300–12310.

[50] E. Vinogradov, P. K. Madhu, S. Vega, *Chem. Phys. Lett.* **2002**, *354*, 193–202.

[51] M. Leskes, P. K. Madhu, S. Vega, *J. Chem. Phys.* **2008**, *128*, 052309.

[52] E. Nimerovsky, R. Gupta, J. Yehl, M. Li, T. Polenova, A. Goldbourt, *J. Magn. Reson.* **2014**, *244*, 107–13.

[53] M. Makrinich, E. Nimerovsky, A. Goldbourt, *Solid State Nucl. Magn. Reson.* **2018**, *92*, DOI 10.1016/j.ssnmr.2018.04.001.

[54] R. D. Shannon, *Acta Crystallogr. Sect. A* **1976**, *32*, 751–767.

[55] M. Bak, J. T. Rasmussen, N. C. Nielsen, *J. Magn. Reson.* **2000**, *147*, 296–330.